Journal of Hydrology 475 (2012) 188–203

Contents lists available at SciVerse ScienceDirect

Journal of Hydrology

journal homepage: www.elsevier.com/locate/jhydrol

A fully coupled numerical modeling for regional unsaturated–saturated water flow

Yan Zhu [a,b], Liangsheng Shi [a], Lin Lin [a], Jinzhong Yang [a,*], Ming Ye [c]

[a] State Key Laboratory of Water Resources and Hydropower Engineering Science, Wuhan University, Wuhan 430072, China
[b] Earth and Environmental Sciences, University of Waterloo, Waterloo, Ontario, Canada N2L 3G1
[c] Department of Scientific Computing and Geophysical Fluid Dynamics Institute, Florida State University, Tallahassee, FL 32306, USA

ARTICLE INFO

Article history:
Received 4 July 2012
Received in revised form 21 September 2012
Accepted 24 September 2012
Available online 6 October 2012
This manuscript was handled by Corrado Corradini, Editor-in-Chief, with the assistance of Christophe Darnault, Associate Editor

Keywords:
Unsaturated–saturated flow
Large-scale water flow simulation
Model verification
Richards' equation
Water balance analysis method

SUMMARY

It is a long-lasting challenge in subsurface hydrologic modeling to develop numerically efficient algorithm for coupling unsaturated and saturated flow, especially in regional-scale modeling. In this study, a new scheme is developed for coupled numerical simulation of unsaturated–saturated water flow at the regional scale. The modeling domain is divided into sub-areas in horizon according to spatially distributed inputs, flow characteristics, and topography conditions. The unsaturated zone of each sub-area is represented by individual one-dimensional soil column. Water balance analysis method is employed to formulate the three-dimensional groundwater model. The unsaturated and saturated zones are implicitly coupled in space and time through the vertical flow between the unsaturated soil columns and the saturated aquifers in that the heads in the unsaturated and saturated zones are integrated in a single matrix equation. The coupling scheme is verified and computational efficiency is evaluated in several hypothetical examples by comparing the simulation results with those of widely used software, including Hydrus1D, SWMS2D, FEFLOW and HydroGeoSphere. In the real-world application, numerical results show that the coupling model can obtain satisfactory simulation results with fairly little computational cost. Compared with existing models, the new numerical scheme is more suitable to regional-scale modeling with complex domain geometry and alternating recharge or discharge fluxes. However, due to the assumptions involved in the method development, the coupling method has its intrinsic limitations and should be used with caution in cases where the lateral flow is predominant in the unsaturated zone.

© 2012 Elsevier B.V. All rights reserved.

1. Introduction

Numerical modeling of water movement in unsaturated soils and saturated groundwater aquifers is crucial for understanding of hydrologic interaction between soil, vegetation, atmospheric processes, and groundwater dynamics in water resource management. A long-lasting challenge in the numerical modeling is to fully couple unsaturated and saturated flows that are controlled by different mechanisms but occur in an integrated hydrologic system. Unsaturated flow is nonlinear in nature and very sensitive to atmospheric changes, soil utilizations, and human activities. As a result, water table, through which the unsaturated and saturated flows are coupled, varies in space and time. Thus, unsaturated–saturated flow processes are complicated and difficult to be described quantitatively and to be solved numerically. The coupled numerical modeling at the regional scale is of particular challenge, due to lack of data to characterize the unsaturated–saturated system, numerical difficulty to solve the governing equations (in particular that of unsaturated flow), and computational burden of model calibration. Therefore, it is important to develop a mathematical/computational method that can efficiently simulate the coupled unsaturated–saturated flow, especially at the regional scale.

This paper presents a numerical method to predict simultaneous responses of unsaturated and saturated flows to changes of hydrologic inputs at the regional scale. The proposed method relies on a new way of coupling unsaturated–saturated flow, and the new coupling method yields satisfactory convergence performance. The proposed method also includes a recently developed numerical scheme of solving groundwater flow equation based on water balance analysis. The numerical scheme is similar to the finite volume methods and is flexible in mesh generation for irregular domain boundaries. Moreover, it is more suitable than other conventional coupled unsaturated–saturated models for modeling systems with complex layering and boundary conditions.

Various models have been developed to simulate the interactions between saturated and unsaturated water flow. The most straightforward approach is to use the three-dimensional (3D) unsaturated–saturated Richards' equation (Freeze, 1971) such as the implementation in the popular software FEFLOW (Diersch and Kolditz, 1998). However, since the 3D unsaturated Richards' equation is highly nonlinear and has to be solved by repetitive iterations, it is not suitable for modeling regional water problems because of its heavy computational burden (Niswonger et al., 2006).

* Corresponding author. Tel.: +86 2768775432; fax: +86 2768776001.
E-mail address: jzyang126@126.com (J. Yang).

0022-1694/$ - see front matter © 2012 Elsevier B.V. All rights reserved.
http://dx.doi.org/10.1016/j.jhydrol.2012.09.048

Nonetheless, a simplification can be made based on the field experiments which show that the lateral hydraulic gradient is usually much smaller than the vertical gradient in the vadose zone at the regional scale (Sherlock et al., 2002). Thus, it is considered to be reasonable for large-scale models to neglect the lateral fluxes while focusing on the vertical fluxes such as evapotranspiration, infiltration, and recharge from the unsaturated zone (Chen et al., 1994). Many studies consider to ignore the 3D variability of the unsaturated system in regional-scale unsaturated–saturated water flow simulation (Harter and Hopmans, 2004; Sheikh and van Loon, 2007; Hunt et al., 2008).

The early simplified coupling unsaturated–saturated models usually also adopted some simplifications to the groundwater flow due to the limitation of numerical simulation techniques, and can only be applied to some specific water flow conditions (Pikul et al., 1974; Feddes et al., 1978; Skaggs, 1978). More recently, with the development of computational sciences, a number of integrated, computationally intensive models, often based on linking an existing vadose zone model and a sophisticated groundwater model, have been developed and applied (Krysanova et al., 2000; Sophocleus and Perkins, 2000). For example, many simplified unsaturated models, such as 1D vertical Richards' equation based unsaturated model (Havard et al., 1994), the conceptual vadose zone model-SVAT (Facchi et al., 2004), the Unsaturated-Zone Flow (UZF1) package (Niswonger and Prudic, 2004) and the Hydrus-based unsaturated flow package (Twarakavi et al., 2008), have been developed or adopted and modified respectively to be combined with MODFLOW (McDonald and Harbaugh, 1988). One superior advantage of the coupling methods based on 1D unsaturated flow and MODFLOW (or other saturated models) is that the computational cost can be reduced significantly by avoiding the non-linear 3D Richards' equation in the unsaturated zone.

Another important issue in coupling models is the numerical scheme for solving the groundwater equation. The most popular schemes are FDM, adopted by MODFLOW, and the finite element method (FEM). However, FDM is not flexible to arbitrary boundary geometries and may lose accuracy when predicting hydraulic heads in the vicinity of irregular boundaries. The only way to fit MODFLOW with arbitrary boundary geometries is by using the mesh refinement, but could greatly increase the computational cost (Spitz et al., 2001; Mehl and Hill, 2004). Moreover, FEM is notorious for its mass imbalance at the local level (Di Giammarco et al., 1996). The finite volume method (FVM) is one of the best algorithms in the sense of easily fitting to irregular geometric boundary while preserving the mass balance well (Erduran et al., 2005; Loudyi et al., 2007). In this study, the groundwater model used in the coupled model is established based on water balance analysis, which is similar to FVM.

2. Methodology

This paper presents a new method for fully-coupled numerical modeling of unsaturated–saturated flow, which is particularly suitable for regional-scale modeling. In the method, the unsaturated–saturated domain is partitioned into a number of sub-areas in horizon mainly according to the spatially distributed inputs (soil material, atmosphere boundary condition, land use, and crop types). In some cases, the sub-area has to be refined according to the specific flow characteristics, which will be demonstrated in Section 5. A 1D soil column is assigned to each sub-area to characterize the average unsaturated water flow in that sub-area. We emphasize that for a regional-scale problem a fully 3D simulation of unsaturated flow is not necessary due to the highly spatial variation of flow parameters. Three assumptions are adopted: (1) there are only vertical exchange fluxes between the unsaturated zone and the saturated zone; (2) a few representative parallel vertical soil columns distributed in horizon are selected to simplify the unsaturated flow simulation; and (3) the possible exchange of flux between representative soil columns is ignored. Under these assumptions, the 1D Richards' equation is employed to represent the unsaturated flow in the representative columns, and then is coupled with a new 3D groundwater flow equation that is formulated using the water balance analysis (Zhu et al., 2010). The unsaturated and saturated modules are integrated by implicitly expressing the vertical flow exchange between the unsaturated and saturated zones. Thus, the head equations for the unsaturated and saturated nodes are assembled together into one matrix, and then solved simultaneously.

This paper elaborates the methodology linking the unsaturated and saturated water flow equations, and several synthetic examples that involve precipitation, evapotranspiration, root uptake, and pumping well are designed to test the performance of the proposed model when handling different water flow conditions. The modeling results are verified by comparing with Hydrus1D, the Variably-Saturated Two-Dimensional Water Flow and Transport Model (SWMS2D), the 3D models HydroGeoSphere (HGS), and FEFLOW. A real case study is also presented to demonstrate applicability of the coupling model in a regional-scale problem with complicated boundary conditions, surface topography and soil characteristics.

3. Coupled modeling of unsaturated–saturated water flow

In this section, the numerical solution of 1D unsaturated flow is first presented, followed by the numerical solution of 3D saturated flow. The coupling between unsaturated and saturated flow is described at the end of this section.

3.1. Numerical solution for 1D unsaturated flow

The vertical flow through the unsaturated zone can be described by Richards' equation as follows (Vogel et al., 1996):

$$\frac{\partial \theta}{\partial t} = \frac{\partial}{\partial z}\left[K(h)\left(\frac{\partial h}{\partial z} - 1\right)\right] - S, \tag{1}$$

where θ is the volumetric water content (volume of water per volume of soil), t is time, $K(h)$ is the unsaturated hydraulic conductivity as a function of pressure head, h is the pressure head, z is the elevation in the vertical direction, and S is the root uptake term (see Section 4), or other source/sink term.

The Galerkin finite element method with linear basis functions is used to obtain the solution of the flow equation subject to the imposed initial and boundary conditions. The detailed derivation can be found in the Hydrus5 manual (Vogel et al., 1996). The final matrix form can be expressed as

$$[P]\{h\}^{k+1} = [E], \tag{2}$$

where $[P]$ is the coefficient matrix in the global matrix equation for water flow, $[E]$ represents the coefficient vector in the global matrix equation for water flow, and superscript $k+1$ denotes the current time level.

3.2. Numerical solution of 3D saturated flow

In this sub-section, the 3D groundwater model is built using water balance analysis method. The new model provides flexibility in simulating the aquifer with irregular shape. The average plane of head gradient in the triangular prism element is defined (see next sub-section), after which the element stiffness matrix is derived by

analyzing the water balance in the control volume. The vertical flow flux is computed using Darcy's law.

Fig. 1 shows the triangular prism $ijki'j'k'$ and the average plane IJK. It can be seen that the x and y coordinates of the three nodes in the average plane IJK equal to those in the upper or bottom surface of the triangular prism $ijki'j'k'$, which can be expressed as $x_I = x_i$, $x_J = x_j$, $x_K = x_k$, $y_I = y_i$, $y_J = y_j$, and $y_K = y_k$. The water balance equation of node i in the saturated zone is given by

$$V_i\mu_i\frac{\Delta H_i}{\Delta t} = Q_i - (q_{i-1/2} - q_{i+1/2})A_i, \tag{3}$$

where μ_i is the elastic storage coefficient; V_i is the control volume of node i; H_i is the hydraulic head of node i; Q_i is the net lateral flux; $q_{i+1/2}$, $q_{i-1/2}$ are the vertical flow fluxes in the upper and the bottom surfaces, respectively; and A_i is the upper surface area of the control volume.

3.2.1. Net lateral flux Qi

In this study, the upper and bottom surfaces of the triangular prism may be tilting. Thus, the vertical velocity exists for all the nodes and the net lateral flux cannot be determined by the head difference of the nodes in the tilted surface. The average plane of head gradient in an irregular triangular prism is defined to approximately calculate the net lateral flux, and the head gradient on this average plane is the average lateral head gradient in this irregular triangular prism element. By assuming that the head varies linearly between the upper and bottom nodes within the element, the vertical position of the average plane of head gradient IJK in the triangular prism $ijki'j'k'$ is given by (Zhu et al., 2010)

$$\bar{z} = \frac{\left\{\frac{1}{12}\left[(z_i - z_j)(z_i + 3z_j) - (z_{i'} - z_{k'})(z_{i'} + 3z_{k'}) + \frac{(z_j - z_{j'})(z_j + z_{j'})}{2} + \frac{(z_{j'} - z_{k'})(z_{j'} + z_{k'})}{2}\right]\right\}}{\left\{\frac{[(z_i - z_j) - (z_{i'} - z_{k'})]}{3} + (z_j - z_{k'})\right\}}, \tag{4}$$

where $z_p (p = i, i', j, j', k, k')$ are the z-coordinates of the triangular prism element nodes and $\bar{z}$ is the z-coordinate of the average plane of head gradient.

The net lateral flux from the plane-IJK to node I is expressed as follows (Zhang, 1983):

$$Q_I = -\frac{T}{4\Delta}\left[(b_i^2 + a_i^2)H_I + (b_jb_i + a_ja_i)H_J + (b_kb_i + a_ka_i)H_K\right], \tag{5}$$

where $H_M (M = I, J, K)$ are the heads of the three nodes on the average plane of head gradient; T is the transmissibility coefficient; Δ is the area of triangle IJK; and a_p, b_p $(p = i, j, k)$ can be expressed as $a_i = y_j - y_k$, $b_i = x_k - x_j$, $a_j = y_k - y_i$, $b_j = x_i - x_k$, $a_k = y_i - y_j$, and $b_k = x_j - x_i$,

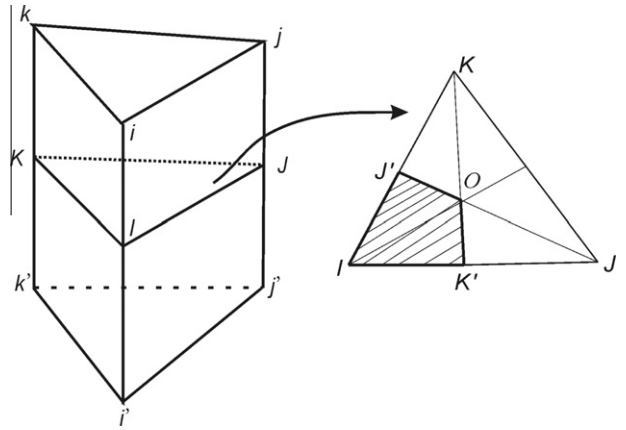

Fig. 1. The triangular prism element $ijki'j'k'$ and the control area (the quadrangle $IK'OJ'$) of node I in the average plane IJK.

where x_p, y_p $(p = i, j, k)$ are the coordinates of each node in the upper surface ijk (Fig. 1).

Since we assume that the head varies linearly with the depth within each prism, the heads of the three nodes on the average plane can be expressed as

$$H_M = \frac{H_p - H_{p'}}{z_p - z_{p'}}(\bar{z} - z_p) + H_p, \tag{6}$$

where H_p and $H_{p'}$ $(p = i, j, k, p' = i', j', k')$ are the heads of the six nodes of the triangular prism element; z_p and $z_{p'}$ $(p = i, j, k, p' = i', j', k')$ $p = i, j, k, p' = i', j', k')$ are the z-coordinates of the six nodes.

In the element $ijki'j'k'$, the lateral flux to node i can be approximated by multiplying the lateral flux to node I and one half the average thickness of the triangular prism element. Thus, the lateral flux to the node i can be expressed as

$$Q_i = -\frac{T}{4\Delta}[(b_i^2 + a_i^2)H_I + (b_jb_i + a_ja_i)H_J + (b_kb_i + a_ka_i)H_K] \tag{7}$$

$$T = \overline{K} \times \overline{B}/2 \tag{8}$$

where $\overline{K}$ is the mean hydraulic conductivity of the triangular prism element and $\overline{B}$ is the mean thickness of the triangular prism element.

Combining Eqs. (6)–(8) gives

$$Q_i = -\frac{\overline{K} \times \overline{B}}{8\Delta}[P_{ii}\beta_I H_i + P_{ii}(1 - \beta_I)H_i + P_{ij}\beta_j H_j + P_{ij}(1 - \beta_j)H_{j'} + P_{ik}\beta_K H_k + P_{ik}(1 - \beta_K)H_{K'}], \tag{9}$$

where

$$\frac{z - z_{i'}}{z_i - z_{i'}} = \beta_I, \quad \frac{z - z_{j'}}{z_j - z_{j'}} = \beta_J, \quad \frac{z - z_{k'}}{z_k - z_{k'}} = \beta_K, \quad a_i^2 + b_i^2 = P_{ii}, \quad a_ia_j + b_ib_j = P_{ij}, \quad a_ia_k + b_ib_k = P_{ik}.$$

3.2.2. Elastic storage Q_μ

The elastic storage characterizes the capacity of an aquifer to release groundwater from storage in response to a decline in hydraulic head. The elastic storage in the control volume of node i can be expressed as

$$Q_\mu = \frac{\Delta}{3}\frac{\bar{\mu}\bar{B}}{2}\frac{\Delta H_i}{\Delta t}, \tag{10}$$

where $\bar{\mu}$ is the average elastic storage coefficient.

3.2.3. Vertical flow flux Q_v

The vertical flow flux to the control volume of node i can be expressed using Darcy's law:

$$Q_v = -A_i(q_{i-1/2} - q_{i+1/2}) = \frac{A_i\overline{K_{i,i-1}}}{B_{i,i-1}}H_{i-1} - \left(\frac{A_i\overline{K_{i,i+1}}}{B_{i,i+1}} + \frac{A_i\overline{K_{i,i-1}}}{B_{i,i-1}}\right)H_i + \frac{A_i\overline{K_{i,i+1}}}{B_{i,i+1}}H_{i+1}, \tag{11}$$

where Q_v is the vertical flux to the control volume of node i; node $i - 1$ and node $i + 1$ are the adjacent nodes to node i in the vertical direction; A_i is the control area of node i in the triangular prism element; $\overline{K_{i,i-1}}$ is the geometric average of hydraulic conductivities in nodes i and $i - 1$; and $B_{i,i-1}$ is the distance between nodes i and $i - 1$. $\overline{K_{i,i+1}}$ and $B_{i,i+1}$ are defined in the same ways.

3.3. Coupled modeling of unsaturated–saturated flow

The soil water model and the groundwater model are coupled by the vertical flow flux from the unsaturated zone to groundwater table, which can be expressed by the head gradient between the adjacent nodes in the unsaturated and saturated zones. Water bal-

ance analysis is implemented to couple the unsaturated equation and 3D groundwater equation. Taking node i, which is adjacent to the groundwater table, for an illustrative example, the control volume of node i is $(z_N - z_{i+1/2})$, as shown in Fig. 2a. We note that for the convenience of derivation of the water equilibrium equation of node i, the control volume of node i is assumed to be $(z_N - z_{i+1/2})$.

In the derivation of the 1D unsaturated model (see Section 3.1), node i is seen to be the node in the bottom boundary of the unsaturated column, which is considered as the zero flux boundary, and the control volume of node i is considered to be $(z_i - z_{i+1/2})$. However, the control volume of node i is assigned to be $(z_N - z_{i+1/2})$ in order to integrate the unsaturated zone and the saturated zone. Moreover, the vertical recharge flux to the groundwater system exists as the bottom boundary for node i. Thus, in the unsaturated model the water flow in the volume $(z_N - z_i)$ and the vertical flow flux q_N (see Fig. 2a) are not considered. The water balance analysis of node i will help to formulate the coupling matrix relating to the unsaturated zone. The water balance equation for node i is expressed as follows:

$$(z_N - z_{i+1/2})\frac{\Delta\theta_i}{\Delta t} = q_{i+1/2} - q_N, \tag{12}$$

where z_N is the elevation of the water table, $z_{i+1/2}$ is the vertical location of the upper surface of unsaturated element, $q_{i+1/2}$ and q_N are the fluxes through the upper and the bottom surfaces, and θ_i is the volumetric water content.

Therefore, the vertical flow flux q_N is expressed as

$$q_N = -\overline{K_{N,i}} \times \frac{H_N - (h_i + z_i)}{z_N - z_i} \tag{13}$$

where $\overline{K_{N,i}}$ is the geometric average of hydraulic conductivities in nodes i and N; h_i represents the pressure head of node i in the unsaturated zone and H_N represents the head of node N at the water table. Thereby, the water balance Eq. (12) can be expressed as

$$(z_N - z_i)C_i(h)\frac{h_i^{j+1}}{\Delta t_j} + \overline{K_{N,i}} \times \frac{h_i^{j+1}}{z_N - z_i} - \overline{K_{N,i}} \times \frac{H_N}{z_N - z_i} + (z_i - z_{i+1/2})\frac{\Delta\theta_i}{\Delta t} = (z_N - z_i)C_i(h)\frac{h_i^{j}}{\Delta t_j} - \overline{K_{N,i}} \times \frac{z_i}{z_N - z_i} + q_{i+1/2}, \tag{14}$$

where $C_i(h)$ is the soil water capacity; $j+1$ and j are the present and previous time. The items $(z_N - z_i)C_i(h)\frac{h_i^{j+1}}{\Delta t_j}$, $\overline{K_{N,i}} \times \frac{z_i}{z_N - z_i}$, $(z_N - z_i)C_i(h)\frac{h_i^{j}}{\Delta t_j}$, $\overline{K_{N,i}} \times \frac{H_N}{z_N - z_i}$, and $\overline{K_{N,i}} \times \frac{-h_i}{z_N - z_i}$ are assembled to generate the global stiffness matrix. The details are presented in the following paragraphs.

Similarly, water balance analysis for nodes at the groundwater surface is carried out to establish the integrated matrix for the saturated zone. Fig. 2b shows the control volume for the node N at the groundwater surface.

The water balance equation for node N is given by

$$V_N\mu_N\frac{\Delta H_N}{\Delta t} = Q_N + (q_N - q_{N-1/2})A_N. \tag{15}$$

For all the nodes at the groundwater surface, the vertical flux q_N is not considered in the 3D groundwater model, which can be expressed as Eq. (13). Then, combined Eq. (13) with Eq. (15) can be obtained as

$$V_N\mu_N\frac{\Delta H_N}{\Delta t} + \overline{K_{N,i}} \times \frac{A_N}{z_N - z_i}H_N - \frac{A_N}{z_N - z_i}h_i = \frac{A_N}{z_N - z_i}z_i + Q_N + (-q_{N-1/2})A_N. \tag{16}$$

By assembling the items $\frac{A_N}{z_N - z_i}z_i$, $\overline{K_{N,i}} \times \frac{A_N}{z_N - z_i}H_N$, and $\frac{A_N}{z_N - z_i}h_i$, the global stiffness matrix of the unsaturated–saturated zone is then formed.

The matrices of the unsaturated and saturated flow can be modified according to Eqs. (14) and (16) to be integrated into one matrix. An illustrative example is given to show the key idea of the coupling procedure. We assume an aquifer with two saturated layers and one 1D unsaturated soil column. The saturated layers are discretized by n nodes in each layer, and the unsaturated column is discretized by m nodes. The global matrix for this aquifer is shown as follows:

$$\begin{bmatrix}
a_1^1 & \cdots & a_1^n & a_1^{n+1} & & & & & & & \\
\vdots & L_1 & \vdots & & \ddots & & & & & & \\
a_n^1 & \cdots & a_n^n & & & a_n^{2n} & & & & & \\
a_{n+1}^1 & & & a_{n+1}^{n+1} & \cdots & a_{n+1}^{2n} & a_{n+1}^{2n+1} & & & & \\
 & \ddots & & \vdots & L_2 & \vdots & & \ddots & & & \\
 & & a_{2n}^n & a_{2n}^{n+1} & \cdots & a_{2n}^{2n} & & & a_{2n}^{3n} & & \\
 & & & a_{2n+1}^{n+1} & & & a_{2n+1}^{2n+1} & A_{2n+1}^N & a_{2n+1}^{3n} & A_{2n+1}^{3n+1} & \\
 & & & & \ddots & & \vdots & L_3 & \vdots & \vdots & \\
 & & & & & a_{3n}^{2n} & a_{3n}^{2n+1} & A_{3n}^N & a_{3n}^{3n} & A_{3n}^{3n+1} & \\
 & & & & & & & A_{3n+1}^N & & A_{3n+1}^{3n+1} & a_{3n+1}^{3n+2} \\
 & & & & & & & & & \vdots & C_1 \quad \vdots \\
 & & & & & & & & & & \cdots \quad a_{3n+m}^{3n+m}
\end{bmatrix}
\begin{bmatrix} H_1 \\ \vdots \\ H_n \\ H_{n+1} \\ \vdots \\ H_{2n} \\ H_{2n+1} \\ \vdots \\ H_{3n} \\ h_{3n+1} \\ \vdots \\ h_{3n+m} \end{bmatrix}
=
\begin{bmatrix} b_1 \\ \vdots \\ b_n \\ b_{n+1} \\ \vdots \\ b_{2n} \\ B_{2n+1} \\ \vdots \\ B_{3n} \\ B_{3n+1} \\ \vdots \\ b_{3n+m} \end{bmatrix}, \tag{17}$$

where the small letters a_i^j, b_i $(i,j = 1,2,\ldots,3n+m)$ represent the original items obtained from the 1D unsaturated water model and the 3D groundwater model, and the capital letters A_i^j, B_i $(i,j = 2n+1, 2n+2, \ldots, 3n+1)$ represent the items that should be modified according to Eqs. (14) and (16).

According to Eq. (14), B_{3n+1}, A_{3n+1}^{3n+1}, A_{3n+1}^N are modified by

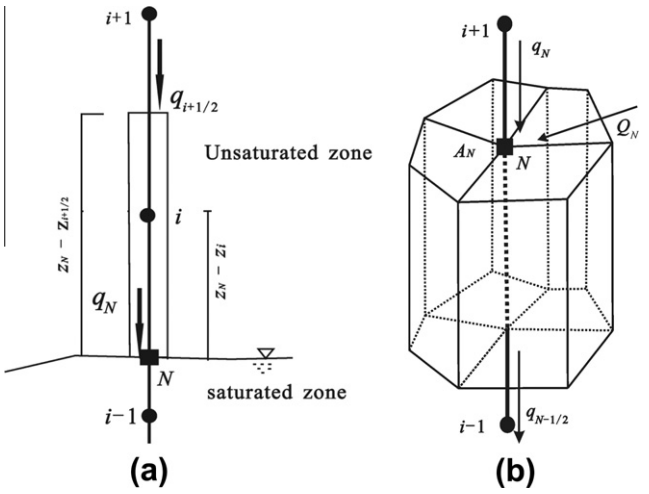

Fig. 2. The control volume of (a) node *i* in the unsaturated zone, and (b) node *N* at the groundwater surface.

Table 1
Input parameters of example 1.

θ_r (−)	θ_s (−)	α (m^{-1})	n (−)	K_S (m/d)
0.057	0.35	4.1	2.28	0.6

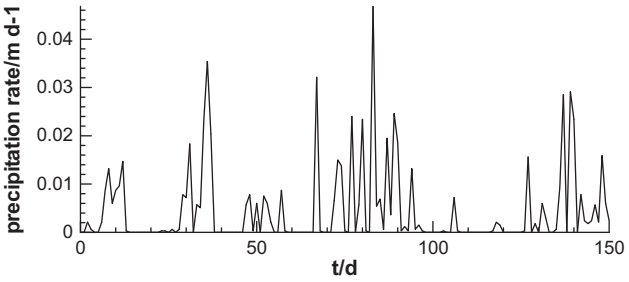

Fig. 3. Daily precipitation rate in example 1.

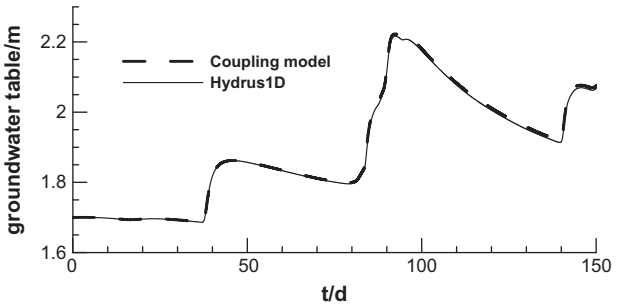

Fig. 5. Comparison of the change process of the groundwater table between the coupling model and Hydrus1D.

$$B_{3n+1} = b_{3n+1} + (z_N - z_{3n+1}) \times \frac{C_{3n+1}(h)h^j_{3n+1}}{\Delta t_j} - \frac{\overline{K_{N,i}} \times z_{3n+1}}{z_N - z_{3n+1}} \tag{18}$$

$$A^{3n+1}_{3n+1} = a^{3n+1}_{3n+1} + (z_N - z_{3n+1}) \times \frac{C_{3n+1}(h)}{\Delta t_j} + \frac{\overline{K_{N,i}}}{z_N - z_{3n+1}} \tag{19}$$

$$A^N_{3n+1} = -\frac{\overline{K_{N,i}}}{z_N - z_{3n+1}} \tag{20}$$

According to Eq. (16), B_p ($p = 2n+1,\ 2n+2,\ldots,3n$), A^{3n+1}_p ($p = 2n+1, 2n+2,\ldots,3n$), A^N_p ($p = 2n+1, 2n+2,\ldots,3n$) are modified by

$$B_p = b_p + \frac{\overline{K_{N,i}}}{z_p - z_{3n+1}} \times z_{3n+1} \times (A_N)_p \tag{21}$$

$$A^{3n+1}_p = -\frac{\overline{K_{N,i}}}{z_p - z_{3n+1}} \times (A_N)_p \tag{22}$$

$$A^N_p = a^N_p + \frac{\overline{K_{N,i}}}{z_p - z_{3n+1}} \times (A_N)_p \tag{23}$$

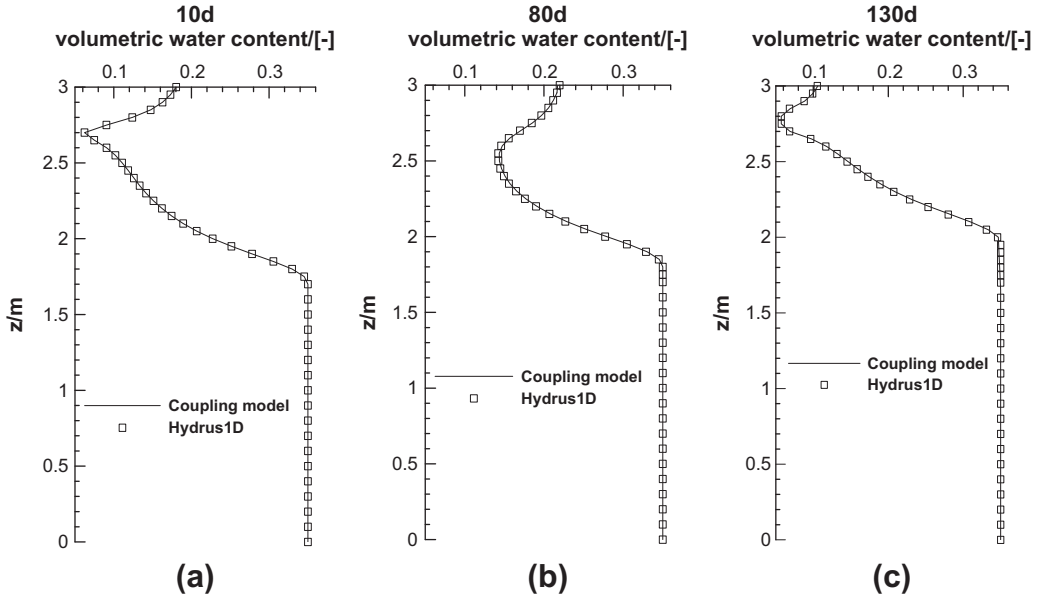

Fig. 4. Comparison of the volumetric water content in the profile between the coupling model and Hydrus1D at different times.

Table 2
Computation times of different models.

Items	Simulation time (s)				
	Coupling model	Hydrus1D	SWMS2D	HydroGeo Sphere	FEFLOW
Example 1	200	7	–	–	–
Example 2	15	–	13	47	–
Example 3	9	–	–	–	137
Example 4	702	–	–	–	–

Table 3
Soil water parameters of example 2.

θ_r (–)	θ_s (–)	α (m^{-1})	n (–)	K_S (m/d)
0.02	0.30	4.1	1.964	0.5

Then, by water balance analysis for the nodes in the unsaturated zone and at the water table, the final global matrix for the subsurface system is thus formed, which can be solved by many sophisticated solvers such as ORTHMIN package (Mendoza et al., 1991).

4. Boundary conditions and source/sink terms

The common boundary conditions (i.e., Dirichlet and Neumann) and source/sink terms (i.e., pumping well and root uptake) are considered as follows:

(1) Dirichlet boundary condition:

$$H_1(x,y,z,t) = \varphi(x,y,z,t)(x,y,z) \in \Gamma_D. \tag{24}$$

(2) Neumann boundary condition:

$$K\frac{\partial H}{\partial n} = q(x,y,z,t)(x,y,z) \in \Gamma_N. \tag{25}$$

(3) Pumping well handled using the distribution rule:

$$Q_i = \frac{L_i K_{ix}}{\sum(L_i K_{ix})} Q_w \beta_l, Q_{i'} = \frac{L_i K_{ix}}{\sum(L_i K_{ix})} Q_w (1-\beta_l), \tag{26}$$

where Q_i and $Q_{i'}$ are the pumping water quantity of the nodes i and i', respectively; L_i is the length of the pumping well filtration in the ith layer and will be changed along with the changing thickness of the saturated layer; and Q_w is the total quantity of the pumping well.

(4) Root uptake:

The sink term of root uptake, S, is defined as the volume of water removed from a unit volume of soil per unit time due to plant water uptake. Feddes et al. (1978) defined S as

$$S = \alpha(h)S_p, \tag{27}$$

where $\alpha(h)$ is a pressure response function of root uptake, and S_p is the potential water uptake by plant, which is related to the potential transpiration rate.

5. Illustrative examples for code verification and application

Some examples are designed to test the accuracy and reliability of the model. The simulation results are compared against the popular models such as Hydrus1D, SWMS2D, FEFLOW, and HGS. The coupling model is also applied to a practical large-scale irrigation district to evaluate the water flow in the sub-surface system with complicated boundary conditions and varying topography. The simulation results are then discussed.

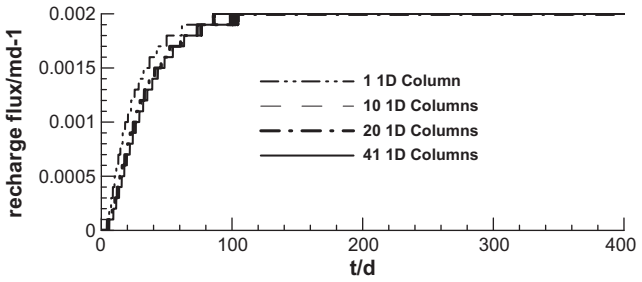

Fig. 7. The change processes of recharge flux to the groundwater at the location of (20,0.5) m.

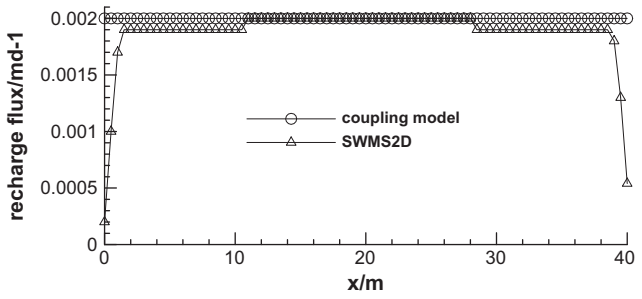

Fig. 8. The flux from the unsaturated zone to the groundwater zone in the steady state.

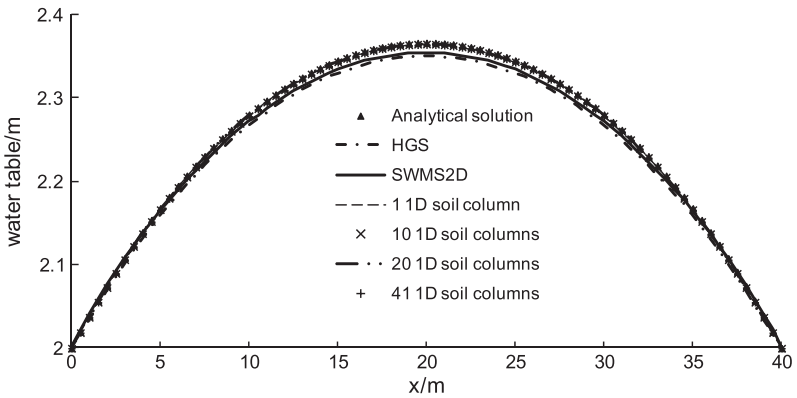

Fig. 6. Comparison of the results of the water table among the coupling model, the analytical solution, HGS, and SWMS2D.

5.1. Example 1: 1D infiltration flow with crop growth

This example considers 1D water flow subject to changing upper boundary condition with crop growth. The soil column is 3 m in length, and the depth of the root zone is 0.3 m. Table 1 lists the flow parameters. Both precipitation and transpiration are applied to the soil surface. Fig. 3 gives the daily precipitation rate at the duration of 150 days. The transpiration rate is assumed to be 0.005 m/d. The column bottom is prescribed as a no-flow boundary condition. The initial water table is located at a depth of 1.3 m from the soil surface. Since the accuracy of our method depends on how precisely we can describe the vertical flow flux between the unsaturated and the saturated zones, the purpose of this example is to test the validity of the coupling process shown by Eqs. (14) and (16) when handling complex boundary conditions (temporally changing precipitation, evapotranspiration, and root uptake).

The water content from the coupling model is compared with that from Hydrus1D, as shown in Fig. 4. The water content in the soil profile changed drastically due to the varying boundary configuration. Moreover, the coupling model is able to capture the flow information in the vertical profile precisely, even in the root zone with much stronger water content change. Fig. 5 shows the transient changing groundwater table from Hydrus1D and the coupling

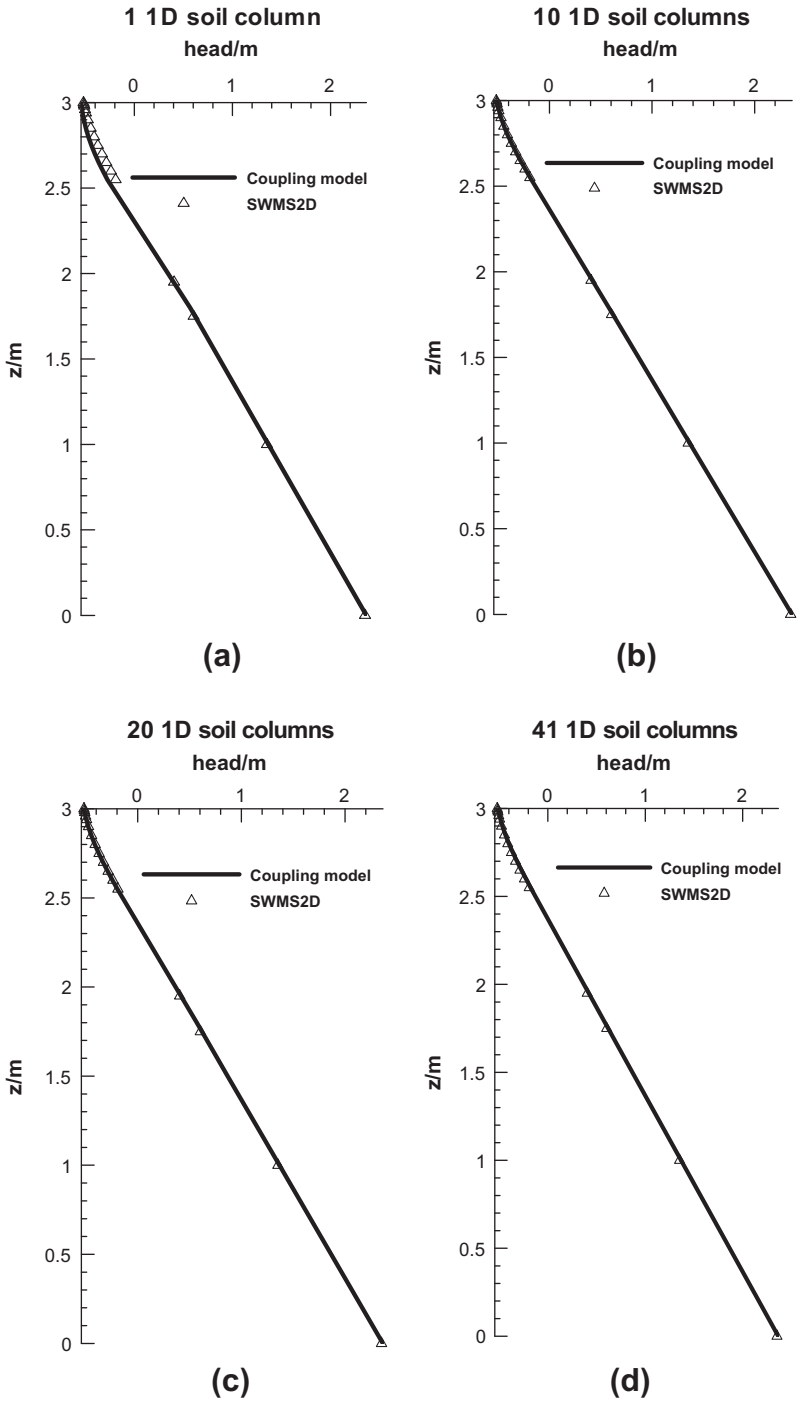

Fig. 9. The comparisons of pressure head calculated from the four assignation plans of the proposed model with that from SWMS2D, respectively.

model. The groundwater table fluctuates due to the temporal change of recharge flux, i.e., during the time when the precipitation rate is smaller than the transpiration rate, the soil is in discharge mode and the groundwater table decreases. In contrast, when the precipitation rate is larger than the transpiration rate, the soil is in recharge mode and the water table rises.

Since in this case the change of head shows strong dependence on the recharge-discharge flux, the good match in Fig. 5 indicates that our method can precisely capture the water exchange between the unsaturated and the saturated zones. It indicates the validity of the coupling method used in this paper, as shown in Eqs. (18)–(23). However, because 3D meshes are used in the saturated zone and consequently much more nodes are calculated in the coupling model, it consumed more simulation time compared with Hydrus1D. The simulation times for our coupling model and Hydrus1D are 200 s and 7 s, respectively (Table 2).

5.2. Example 2: 2D water flow

In this example, the coupling model is used to simulate the water flow between two rivers prescribed as constant-head boundary conditions of the modeling domain. Constant precipitation infiltration of 0.002 m/d is imposed at the top. The distance between the rivers is 40 m. The soil profile is 3 m in depth. Table 3 presents the soil water parameters. The steady-state head at location x (originating from the left boundary) is given by the analytical solution (Bear, 1972)

$$H(x)^2 = (H_1)^2 + \frac{(H_2)^2 - (H_1)^2}{l}x + \frac{W}{K}(lx - x^2), \tag{27}$$

where $H(x)$ is the head; H_1, H_2 are the heads at the left and right boundary; l is the distance between the two rivers; W is the precipitation rate; and K is the saturated hydraulic conductivity.

Since the vertical flux from the unsaturated zone to the saturated zone is equal to the precipitation rate when the groundwater system is in steady state, theoretically we can use one soil column to represent the vertical water exchange between the unsaturated and the saturated zones in steady state. However, during the tran-

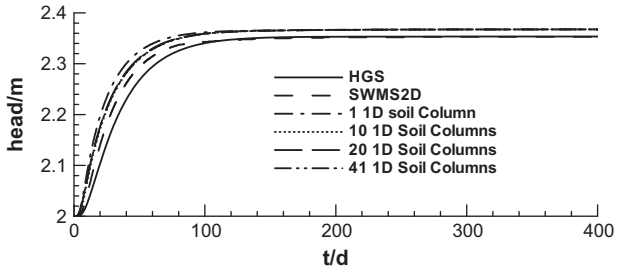

(a) At the location of node (20, 0.5, 2.0) m

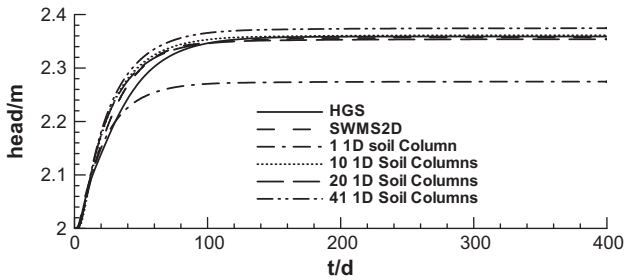

(b) At the location of node (20, 0.5, 2.55) m

Fig. 10. Comparison of the head change processes from the results of the four assignation plans of the coupling model and SWMS2D.

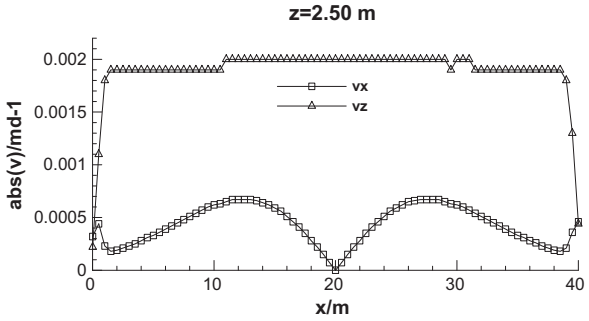

(a) The segment from (0, 0.5, 2.5) m to (40, 0.5, 2.5) m

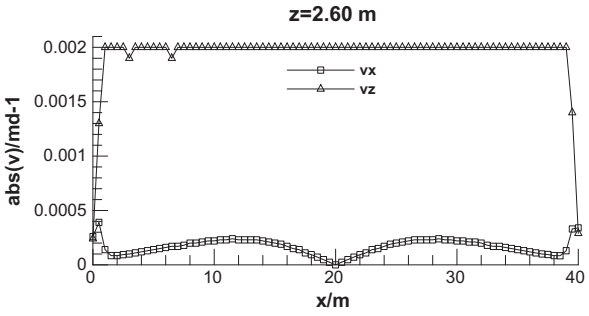

(b) The segment from (0, 0.5, 2.6) m to (40, 0.5, 2.6) m

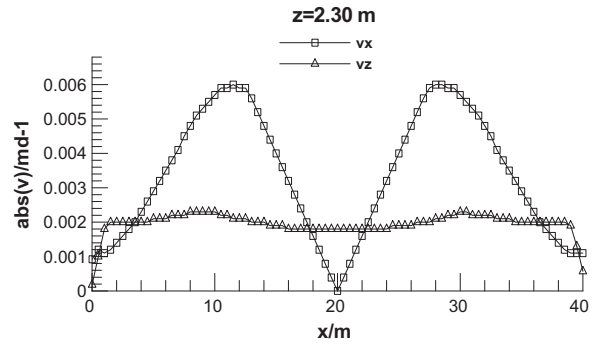

(c) The segment from (0, 0.5, 2.3) m to (40, 0.5, 2.3) m

Fig. 11. The compariosn of the vertical velocity and the lateral velocity distribution in different segments.

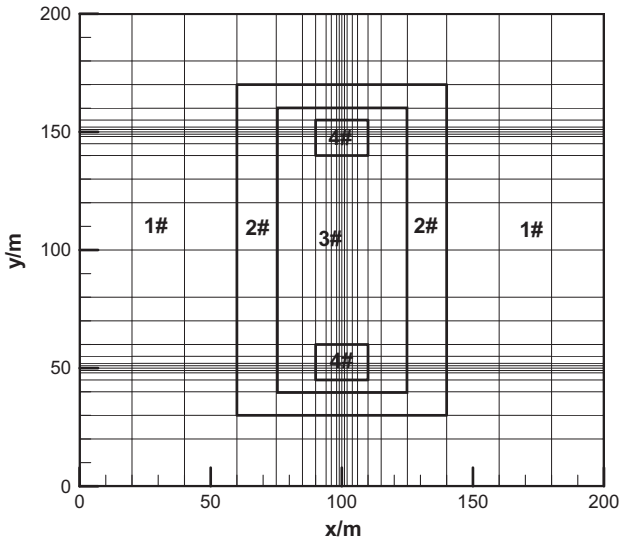

Fig. 12. The elements and the distribution of the 1D columns.

Table 4
Soil water characteristic parameters of example 3.

θ_r (−)	θ_s (−)	α (m^{-1})	n (−)	K_S (m/d)
0.02	0.3	4.1	1.964	7.4

sient stage the vertical fluxes may vary at different locations along x direction, and then insufficient soil columns could lead to deviated estimation to the real water flux. To detect the influence from the estimation of vertical fluxes, we investigate the unsaturated–saturated flow under four different configuration schemes: 1 column (scheme 1), 10 columns (scheme 2), 20 columns (scheme 3), and 41 columns (scheme 4). SWMS2D and HGS are run to verify the results.

Fig. 6 plots the water tables solved with four different schemes using the coupling model and compared with SWMS2D, the analytic solution, and HGS in the steady-state. A small deviation can be found between the results from the coupling model and SWMS2D and HGS, the reason for which will be explained later. However, no obvious difference can be found for the water tables solved by the four soil column schemes. As stated before, in steady state the recharge flux from the unsaturated zone to the groundwater system is equal to the precipitation rate, no matter how many soil columns are used and no matter how and where these columns are placed. Fig. 7 shows the transient recharge fluxes to the groundwater system under the four schemes. Although scheme 1 with one soil column leads to the overestimation of the flux during the transient stage, it still can reach accurate steady-state flux.

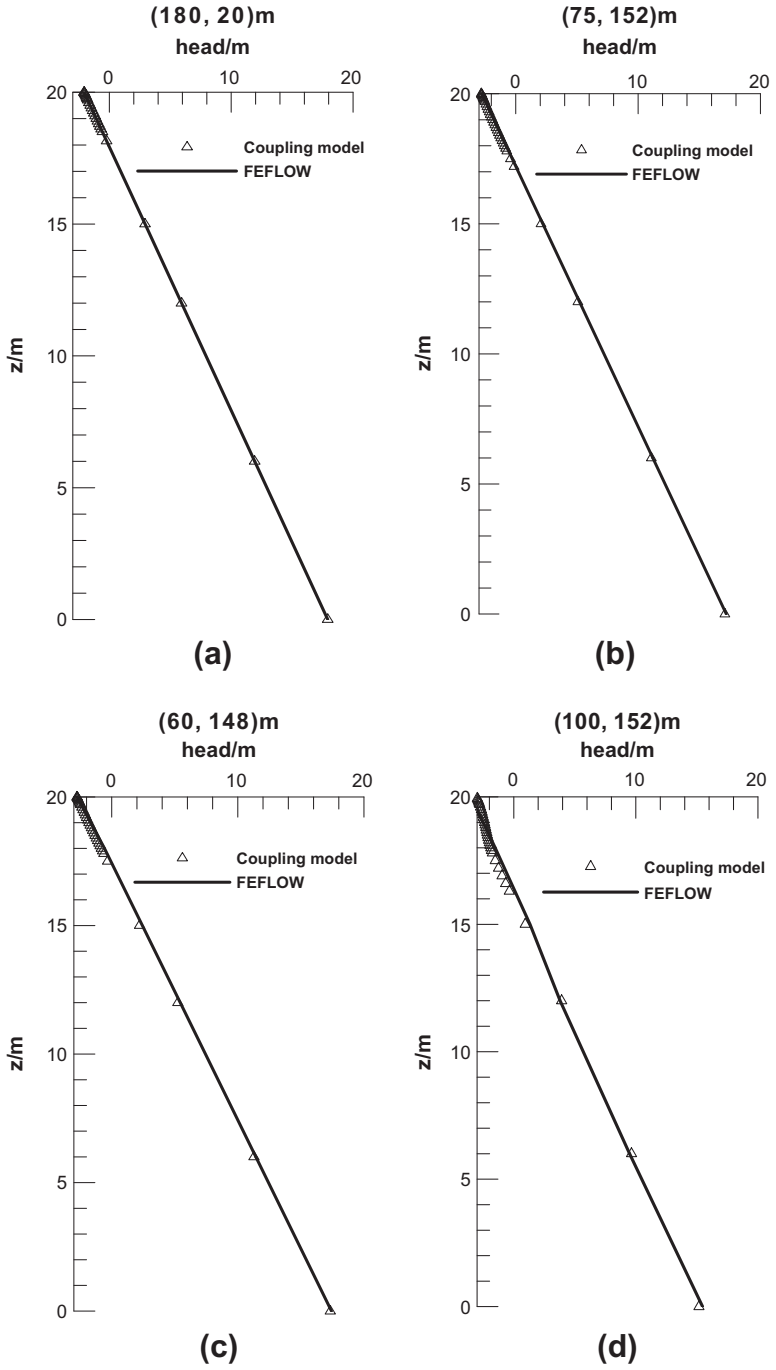

Fig. 13. The comparison of pressure head profiles from the coupling model and FEFLOW at the locations of the four 1D representative columns.

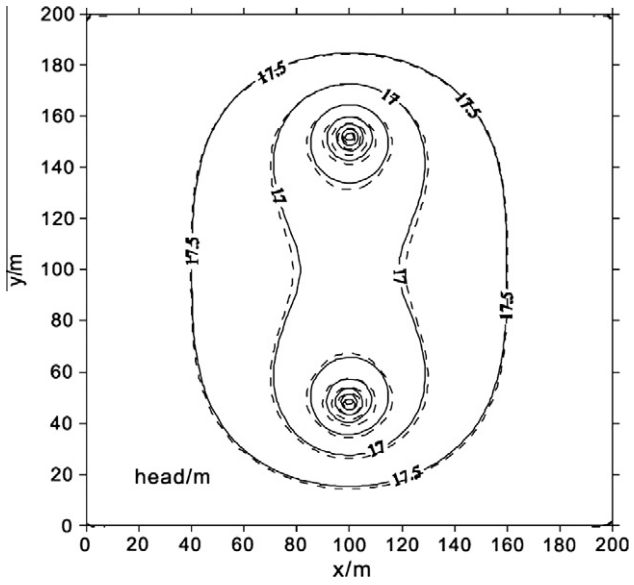

Fig. 14. Comparison of water head contour simulated by the proposed model (dotted line) and FEFLOW (solid line) at the plane of $z = 6$ m.

Additional columns (schemes 2–4) are able to accurately receive the recharge fluxes from the unsaturated zone. This could be the main reason why the simulated water tables are in the same position for these four different schemes.

In Fig. 6, a small deviation can be found between the results from the coupling model and SWMS2D and HGS, which could be explained by the minor difference of the vertical recharge flux. As SWMS2D is a fully 2D water flow model, it is difficult to output the transient recharge flux automatically. Thus, we only compare the calculated recharge fluxes between the two models in the steady state, which can be seen in Fig. 8. It seems our method generates satisfactory fluxes except near the left and right boundaries, where the recharge is a little higher than that from SWMS2D. This could be why the water table obtained by the coupling model is a little higher than that from SWMS2D.

Fig. 9 presents the steady-state head distribution along the segment from (20, 0.5, 0.0) m to (20, 0.5, 3.0) m under the four different soil column schemes. The heads in the saturated zone under the four schemes do not show any difference due to spatially constant recharge, while a slight discrepancy in the unsaturated zone can be observed if only one soil column is assigned. Under the one-soil-column scheme, the column places at $x = 10$ m; it barely represents the flow characteristics in the zone far from $x = 10$ m, and one column is too sparse to characterize the flow characteristics in the unsaturated zone. Additional columns (scheme 2 with 10 columns) are able to capture the transient flux accurately. Fig. 10 plots the transient heads at one saturated point (20, 0.5, 2.0) m and one unsaturated point (20, 0.5, 2.55) m. The simulation error in the unsaturated zone decreases from 0.08 m with one soil column to 0.001 m with 10 soil columns or more columns. However, it seems that the improvement for the simulation accuracy is not significant in the saturated zone.

In our method, we ignore the water exchange between the soil columns and assume that the possible lateral water exchange be-

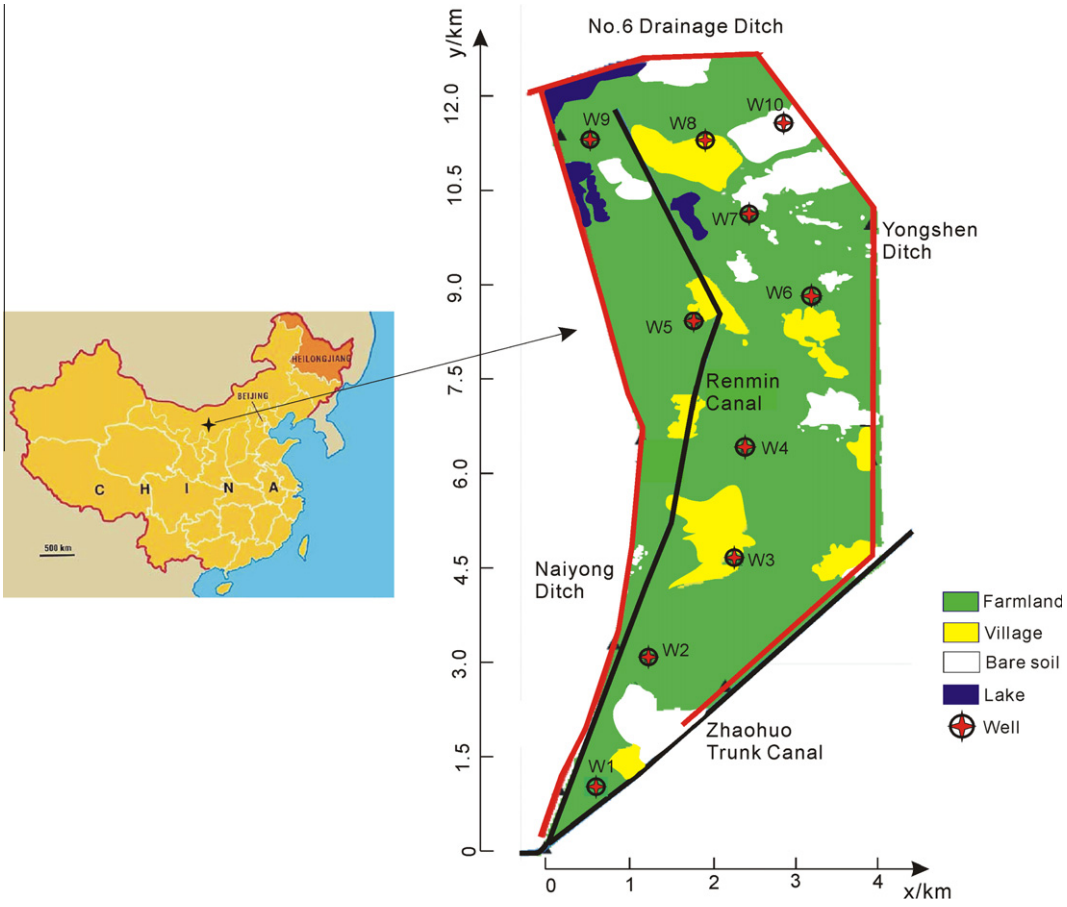

Fig. 15. Simulation domain.

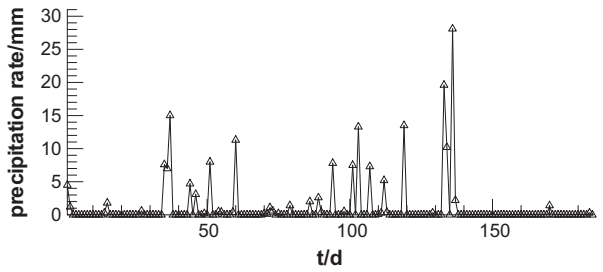

(a) Daily precipitation rate

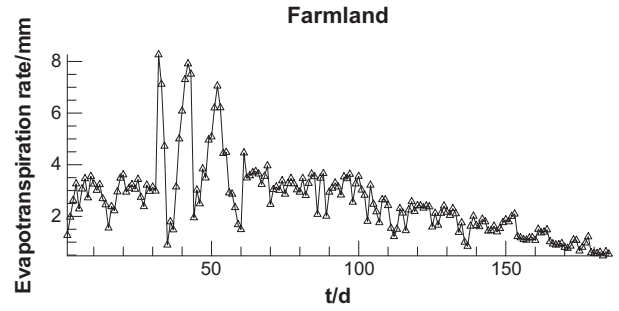

(b) Evapotranspiration in farmland

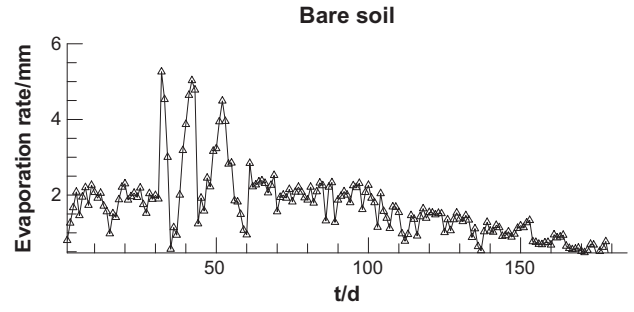

(c) Evaporation in bared soil

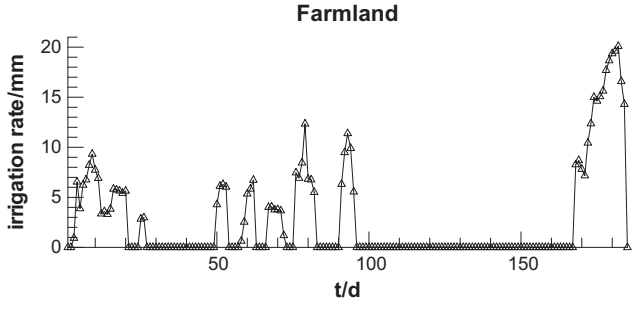

(d) Irrgation rate in farmland

Fig. 16. Daily climate data in Yonglian Irrigation District.

tween the unsaturated and the saturated zones can be neglected. This example seems fitting the assumption by examining Fig. 11a and b, where the real vertical and lateral flux (calculated by SWMS2D) of the segments from (0,0.5,2.5) m to (40,0.5,2.5) m and from (0,0.5,2.6) m to (40,0.5,2.6) m are plotted. As the figures show, the lateral flux is much smaller than the vertical flux, except in the vicinity of boundaries. In this example, the thickness of the vadose zone is fairly small. Larger adverse influences for ignoring the lateral flow could be produced in the deep soil, which has been investigated by Sheikh and van Loon (2007) and Hunt et al. (2008). We also notice that the assumption on ignoring the lateral water exchange between the unsaturated and the saturated zones is somewhat strong. The lateral water flux at x = 10 m, 30 m (where the water table locates in this case) in Fig. 11c is large. It also attributes to the mismatch between the results from our coupling model and SWMS2D and HGS (shown in Figs. 6 and 9). Thus, it could conclude that the assumption may lead to considerable error when the lateral flux grows dominant in the unsaturated zone.

Where the simulation costs of the three models are concerned, it costs the coupling model 15 s for the four schemes respectively, 13 s for SWMS2D, and 47 s for HGS with almost the same time steps (Table 2). In this example, the simulation costs do not increase with the increasing number of the 1D soil columns. The reason could be that the number of the soil columns is not large enough to induce an obvious simulation cost. The simulation cost of the coupling model is a little larger than that of SWMS2D, but can save simulation cost obviously compared with the fully 3D model.

Three conclusions may be drawn from the analysis of this example. Firstly, how to partition the sub-area is mainly controlled by the upper conditions and the change of the hydraulic gradient. Using one sub-area partitioned by the upper conditions may lead to the exact simulation results in the saturated zone but bring errors in the unsaturated zone. Using more sub-areas divided according to the hydraulic gradient will improve the simulation accuracy for the nodes in the unsaturated zone. Secondly, if the recharge flux can be estimated exactly, the number and the locations of the 1D soil columns cannot affect the simulation results in the saturated zone seriously in this example. Actually, in field situations with low water table gradients, lateral unsaturated flow can be probably negligible (Pikul et al., 1974). Thus, using a 1D vertical equation to represent the water flow in the unsaturated zone is reasonable. Thirdly, using the coupling model to the area with great lateral flow, like the area near the left and right boundaries in this example, could induce a non-negligible simulation error and a rigorous model could obtain more accurate results.

5.3. Example 3: water flow with pumping well

A 3D aquifer with the size of 200 m × 200 m × 20 m is considered. Two pumping wells with the same pumping rate of 500 m^3/d are located at (100,48) m and (100,152) m, respectively. The initial head is 18 m for the whole region. All four lateral boundaries are with a constant head of 18 m, and the bottom consists of no-flow boundaries. Four 1D soil columns are assigned to represent the unsaturated zone according to the approximate estimate of

Table 5
Soil water characteristic parameters of example 4.

Depth (m)	θ_r (–)	θ_s (–)	α (m^{-1})	n (–)	K_S (m/d)
0–7	0.065	0.41	7.5	1.89	1.06
7–53	0.057	0.41	12.4	2.28	3.50

Table 6
Water table observation values on May 1, 2004.

Well number	x (m)	y (m)	Water table (m)
1	560	1040	1026.521
2	1308	3170	1025.594
3	2520	4430	1025.334
4	2340	6070	1025.065
5	2010	8160	1024.78
6	3390	8360	1024.428
7	2790	9660	1024.607
8	1950	10,820	1024.313
9	1030	11,155	1024.402
10	2950	11,090	1024.312

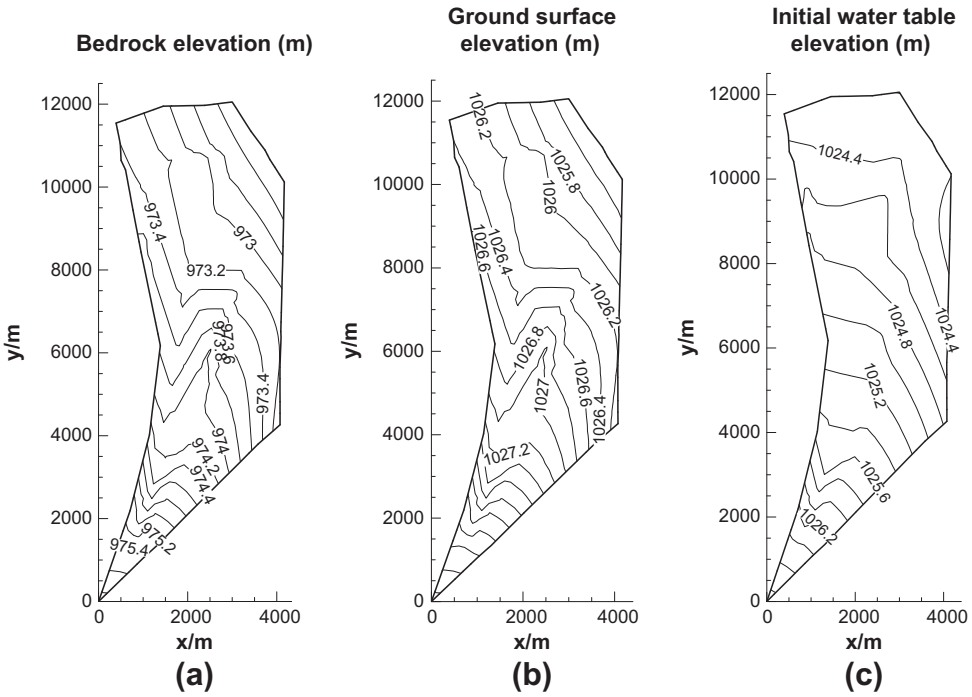

Fig. 17. (a) Bedrock elevation, (b) ground surface elevation, and (c) initial water table elevation.

Table 7
The input information.

Items	Values	
	In the saturated zone	Each 1D soil column
Number of nodes (one layer)	730	–
Number of elements (one layer)	1336	–
Number of 1D soil columns	–	3
Number of layers in *z* direction	12	500
Layers thickness in *z* direction	5.0 m (except the bottom layer and the upper layer)	0.1 m (except the bottom layer)
Initial time step	0.001 d	
Multiplication factor	1.2	
Max time step	0.1 d	
Simulation time	185 d	

the hydraulic gradient, as shown in Fig. 12. Table 4 lists the flow parameters.

Fig. 13 shows the heads of all the representative 1D columns from the coupling model and FEFLOW, and Fig. 14 gives the head contours comparison between the two models. In this example, the actual soil flow exists in all the three directions in the unsaturated zone. The simulation accuracy is supposed to be sacrificed by only considering the vertical flow. However, the coupling model can produce the unsaturated heads well (simulation error is less than 0.002 m) and the simplification to unsaturated flow did not lead to obvious deviations to the real head.

The number of nodes is greatly decreased due to the simplification of the unsaturated zone. There are 23,345 nodes for FEFLOW modeling, whereas there are 4118 nodes for our proposed model. The computational time is 9 s for our proposed model against 137 s for FEFLOW (Table 2). The coupling model enhances the simulation efficiency significantly compared with the fully 3D model.

In this example, the groundwater table changes abruptly and strongly. However, the coupling model can obtain the hydraulic head accurately in the saturated zone. Even for the nodes in the unsaturated zone, using a limited number of 1D soil columns can lead to reasonable simulation results. Furthermore, the coupling model uses much fewer nodes in the unsaturated zone than the fully 3D model does, and this decreases the simulation burden significantly.

5.4. Example 4: water flow simulation in Yonglian Irrigation District

After testing the validity and the efficiency of the coupling model, we further apply it to a practical district, the Yonglian Irrigation District, Inner Mongolia, China (Fig. 15). The Yonglian Irrigation District has an area of approximately 29.1 km^2 and is representative of agricultural and irrigation practices in Hetao Irrigation District. The ground surface elevation decreases from 1028.9 m to 1025.4 m from the southwest to the northeast. This irrigation district has well-defined hydrogeological borders by the channel network, represented by the no. 6 Drainage Ditch and Yongshen Ditch in the northeast and the Zhaohuo Trunk Canal and Naiyong Ditch in the southwest (Fig. 15). The irrigation water is supplied from the Zhaohuo Trunk Canal in the southwest. There is water existing in the Yongshen Ditch for the whole year in the northeast. Thus, the first-kind boundary condition is applied to these two segments and the non-flow boundary conditions for the other segments of the district.

In this irrigation district, different land and crop types are distributed randomly, so it is hard to rigorously partition the domain

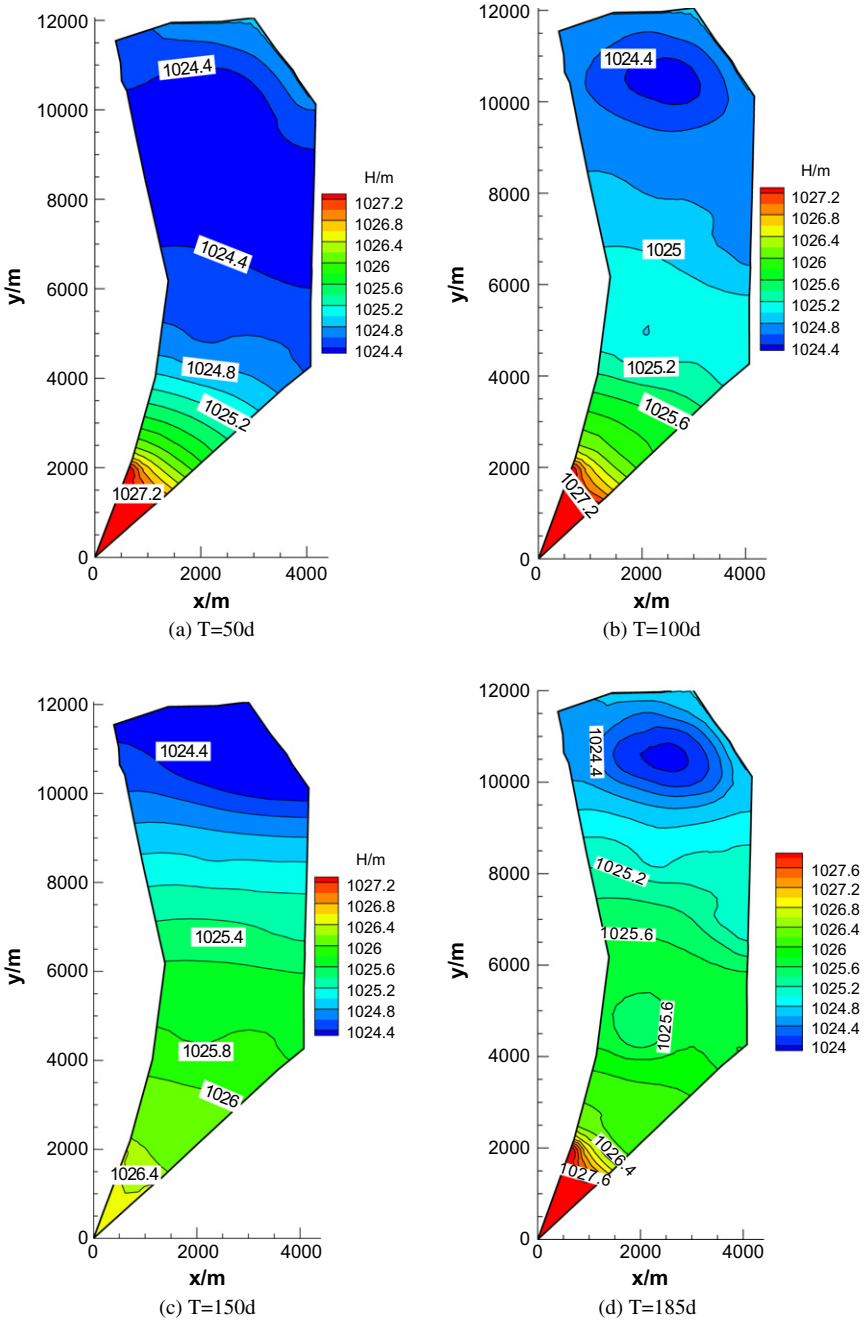

Fig. 18. Simulated water table at output times.

into sub-areas in the horizontal plane. In general, we coarsely divide the domain into three sub-areas according to land type: farmland, villages, and bared soil. The assumptions here are that the area of the lake is small and classified as bared soil, and the crop types in the farmland are not further distinguished. The daily rainfall rate for the whole domain is the same, as shown in Fig. 16a. However, each sub-area has its own evapotranspiration rate, as seen in Fig. 16b and c. The reference evapotranspiration rate is calculated by Penman–Monteith equation, and then multiplied with the crop coefficient to obtain the potential evapotranspiration rate (Li, 2009). The irrigation water is only applied to the farmland, as shown in Fig. 16d. There is no measured evaporation data for the villages, and it is set as the same with that in the bared soil in the simulation. The upper boundary conditions of the domain are set as the atmospheric boundary conditions with the specific rainfall rate, evapotranspiration rate, and irrigation rate for different land types.

From the hydrogeological characteristics of the study area provided by the Geological Department of Inner Mongolia, the subsurface system of the domain could be divided into six aquifers within the depth of 100 m. The top aquifer within the depth of 7 m is loamy sand with lower hydraulic conductivity, and an underlying sand aquifer with the thickness of 46 m has higher penetrability, which is lying on an impervious clay layer with 1 m. From the depth of 54–88 m, it is a fine sand aquifer, and from 88 m to 93 m a clay layer, lying on pervious substrata of fine sand from the depth of 93 m to 100 m. Because of the existence of the clay aquifer in the depth of 54 m and the shallow depth of the groundwater table, we use the clay aquifer as the bottom of the simulation domain. Based on the hydrogeological characteristics,

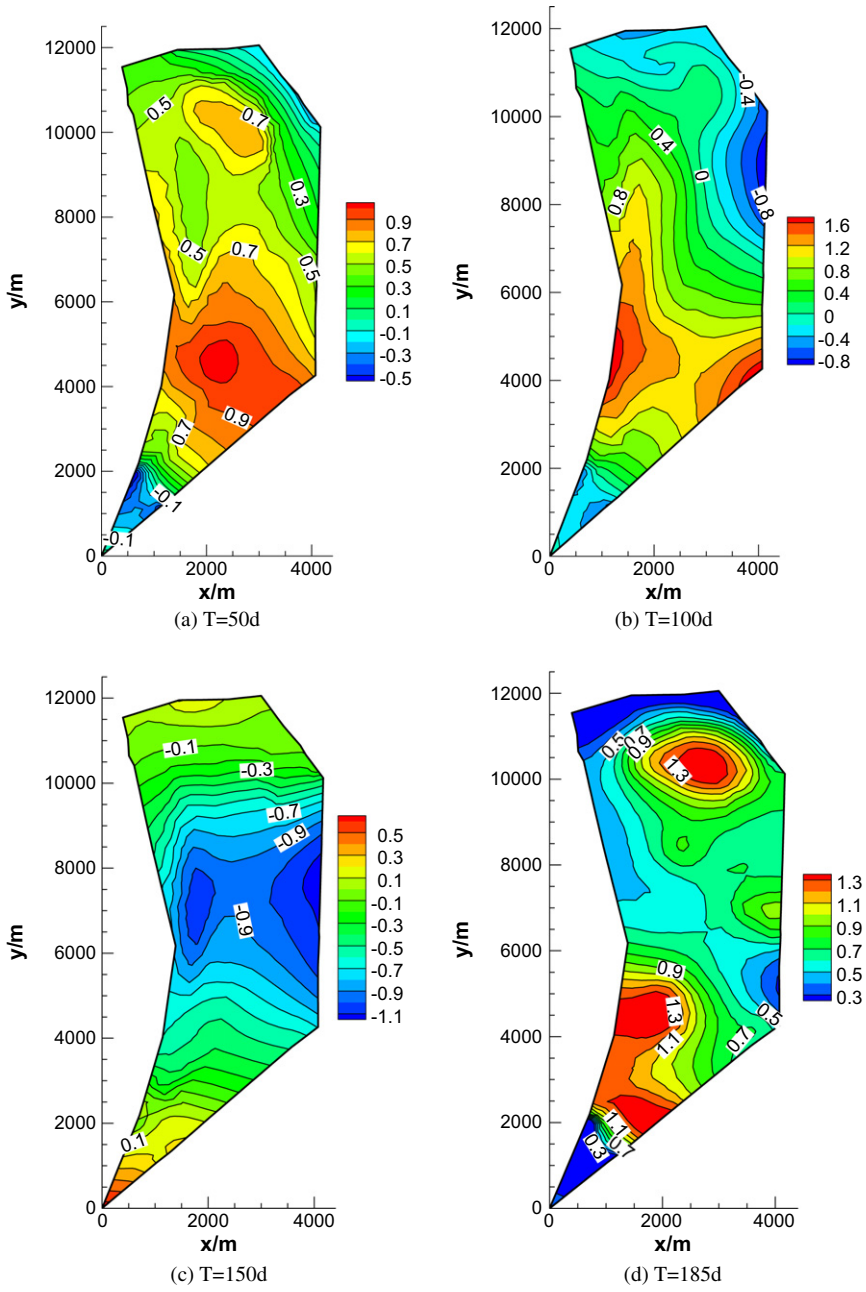

Fig. 19. Difference between simulated and estimated water table surface at different output times.

the domain can be treated as two layers: sandy loam and fine sand. The van Genuchten model is used to represent the unsaturated hydraulic conductivity and water content dependency on the capillary pressure (van Genuchten, 1980). The van Genuchten parameters for sandy loam and loamy sand suggested by Carsel and Parrish (1988) are used for the two layers (Table 5). Note that the layers should be refined to guarantee simulation accuracy. The details of the layer information can be seen in the subsequent section.

Ten observation wells were set in this district, the groundwater tables of which were observed every 6 days from April 2004 to December 2005. The initial hydraulic head of the domain was set according to the interpolation of the observation values of the ten wells on May 1, 2004 (Table 6). Similarly, the elevation of the ground surface was interpolated by the elevations of the ten observation wells. Fig. 17a–c shows bedrock elevations, ground surface elevations, and initial water table elevations of the study area, respectively.

The software FEFLOW is used to generate the node, mesh, and boundary condition information. A FORTRAN package is programmed to transfer the output files from FEFLOW to the required input files of the coupling model. Table 7 lists the general input information.

The simulation was run from May 1, 2004 to November 1, 2004, lasting for 185 days. Fig. 18a–d shows the simulated water table in different output times. It can be seen that the predominant flow direction is from southwest to northeast. The water table distribution has a general rise tendency from the 50th day to the 100th day, which can be seen in Fig. 18a and b, mainly due to the vertical recharge from irrigation water, as in Fig. 16d, and the lateral recharge from the southwest boundary. The similar changing tendency of the water table can be observed comparing Fig. 18c with Fig. 18d. Thus,

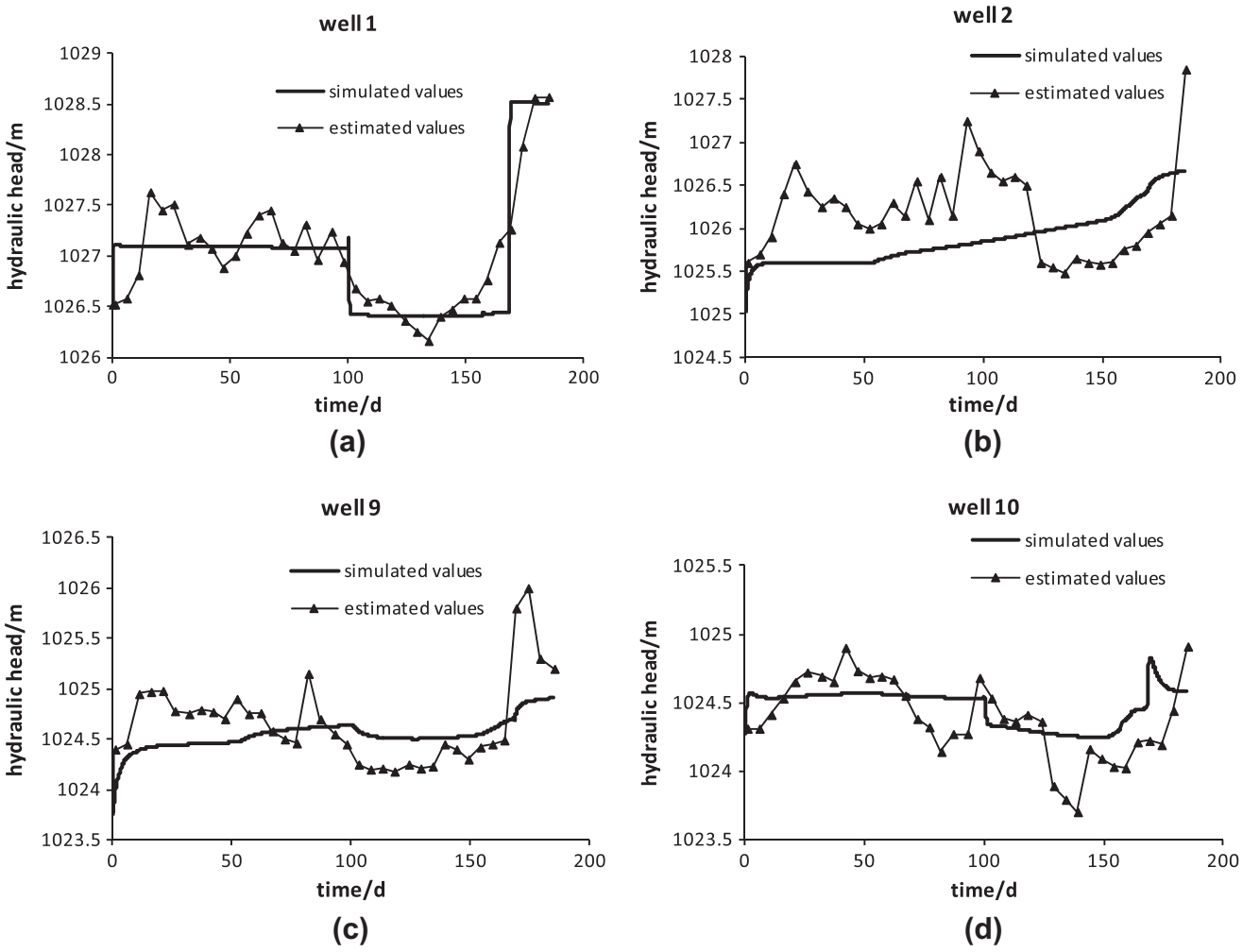

Fig. 20. Comparison between simulated and estimated hydraulic head values at (a) well 1, (b) well 2, (c) well 9, and (d) well 10.

Table 8
The recommended computer specifications at a minimum.

Item	Processor (GHz)	Hard disk size (GB)	Memory (GB)	Graphics	Monitor
Recommended value	2	40	2	Highest color of 32 bit	1024 × 768

the model works well to show the variation of the hydraulic head along the complicated boundary conditions and water supply.

Fig. 19a–d further shows the difference between the estimated values with the simulated values. The estimated water table values in the domain are obtained by interpolation of the estimated values of the ten observation wells. The differences are mainly lower than 1.0 m, as shown in Fig. 19. At the end of simulation time (t = 185 d), there is an abrupt rise of the water table observed at all the observation wells caused by irrigation (Fig. 20). However, the model is not sensitive enough to report this strong instant change of water table, which results in the larger differences of water table in the end, as shown in Fig. 19d. The differences may be attributed to the delayed effect of the recharge from the upper boundary in the unsaturated zone and the inadequacy of observation values used to interpolate the water table in the domain.

Fig. 20 shows the temporal patterns of estimated and simulated heads in well 1, well 2, well 9 and well 10. These four wells are near the boundaries and well 10 is located in bared soil. Another three wells are located in farmland. In general, the simulated heads do not change as sensitively as the estimated values, but still can keep the simulation accuracy in a relative high level, especially for the nodes near the boundaries, which are influenced by the lateral boundary conditions significantly.

The computational time needed to perform the calculation is of paramount importance for the coupling model, because it seriously affects its applicability to regional scale problems. This example was run on a 2.75 GB RAM, double 3.60 GHz Pentium CPU–based personal computer. It costs the coupling model 702 s to perform this case with 1876 time steps (Table 2).

In this example, the domain is divided in horizon based on the land type, but the influence of the ground surface elevation and the ground water table is ignored. It would take errors to the simulation results by using one 1D soil column to represent the water flow of the sub area with an average surface elevation. However, the varieties of the ground surface elevation and the water table are small values via the lengths of the domain in the horizontal directions in this example. Otherwise, the ground surface elevation and the water table heads should be considered together to create the sub-areas. Work is ongoing to estimate the applicability limita-

tion of the coupling model and to test how the division schemes of the sub-areas affect the simulation accuracy.

6. Conclusions

Precise solutions for the combined saturated and unsaturated flow usually resort to very fine spatial and temporal discretization, and the computational cost grows fast as the simulation scale becomes large. In this paper, a new fully coupling model has been proposed for unsaturated–saturated water flow. The coupling method and four examples are elaborated in details. The model can be run with the operating system Windows at most personal computers, and the recommended computer specifications have been listed in Table 8.

Some conclusions can be drawn from this work, as follows:

(1) The exchange flux between the vadose zone and the groundwater system is an important indicator to estimate the performance of the coupling technique. The accurate capture of the change of the water tables in the testing examples 1, 2 and 3 (Sections 5.1–5.3) could demonstrate the validity of the model to obtain the accurate recharge/discharge flux.
(2) The model is applied to a practical irrigation district to estimate the water flow with complex boundary conditions and varying topography after being validated as an accurate model. Reasonable simulation results are obtained by using a limited number of 1D soil columns with small computational cost. The model shows great applicability potential to complicated large-scale unsaturated–saturated water flow problems.
(3) The boundary conditions, hydraulic gradient and ground surface elevations are important factors to be considered when partitioning the unsaturated zone in horizon. The assignation of the 1D columns affects the simulation results of the unsaturated zone more than that of the saturated zone. More 1D columns will help to increase the simulation accuracy in the unsaturated zone.
(4) The simplifications to the unsaturated zone greatly reduce the number of nodes in the unsaturated zone and simplify the simulation processes, which contribute to reduce the computational burden significantly, especially for large-scale 3D unsaturated–saturated water flow problems.
(5) It should be noted that the coupling model should not be used in problems where the lateral flow is predominant in the unsaturated zone because of the assumptions used in this paper.

Acknowledgments

The study was partially supported by the National Basic Research program of China (No. 2010CB42880204), Natural Science Foundation of China through Grants 51079101, 51009110, and 41072189, PhD candidates' self-research program of Wuhan University in 2008 and Scholarship Award for Excellent Doctoral Student granted by the Ministry of Education.

References

Bear, J., 1972. Dynamics of Fluid in Porous Media. Elsevier, New York, NY.
Carsel, R.F., Parrish, R.S., 1988. Developing joint probability distributions of soil water retention characteristics. Water Resour. Res. 24, 755–769.
Chen, Z., Govindaraju, R.S., Kavvas, M.L., 1994. Spatial averaging of unsaturated flow equations under infiltration conditions over areally heterogeneous fields—1. Development of models. Water Resour. Res. 30 (2), 523–534.
Di Giammarco, P., Todini, E., Lamberti, P., 1996. A conservative finite elements approach to overland flow: the control volume finite element formulation. J. Hydrol. 175 (1–4), 267–291.
Diersch, H.J.G., Kolditz, O., 1998. Coupled groundwater flow and transport: 2. Thermohaline and 3D convection systems. Adv. Water Resour. 21 (5), 401–425.
Erduran, K.S., Ilic, S., Kutija, V., 2005. Hybrid finite-volume finite-difference scheme for the solution of Boussinesq equations. Int. J. Num. Meth. Fluids 49, 1213–1232.
Facchi, A., Ortuani, B., Maggi, D., Gandolfi, C., 2004. Coupled SVAT–groundwater model for water resources simulation in irrigated alluvial plains. Environ. Model. Softw. 19 (11), 1053–1063.
Feddes, R.A., Kowalik, P.J., Zaradny, H., 1978. Simulation of Field Water Use and Crop Yield. John Wiley & Sons, New York, NY.
Freeze, R.A., 1971. Three-dimensional, transient, saturated–unsaturated flow in a groundwater basin. Water Resour. Res. 7 (5), 153–171.
Harter, T., Hopmans, J.W., 2004. Role of Vadose zone flow processes in regional scale hydrology: review, opportunities and challenges. In: Feddes, R.A., de Rooij, G.H., van Dam, J.C. (Eds.), Unsaturated Zone Modeling: Progress, Applications, and Challenges. Kluwer, pp. 179–208.
Havard, P.L., Prasher, S.O., Bonnell, R.B., Madani, A., 1994. LINKFLOW, a water flow computer model for water table management: part I. Model development. Soil Water Div. ASAE 38 (2), 481–488.
Hunt, R.J., Prudic, D.E., Walker, J.F., Anderson, M.P., 2008. Importance of unsaturated zone flow for simulating recharge in a humid climate. Ground Water 46 (4), 551–560.
Krysanova, V., Wechsung, F., Arnold, J., Srinivasan, R., Williams, J., 2000. SWIM (Soil and Water Integrated Model), User Manual. PIK Report Nr. 69.
Li, H.Y., 2009. Study on the Water and Salt Dynamics of Irrigation District-Yonglian Experiment Area as Example. MA Thesis. Wuhan University (in Chinese).
Loudyi, D., Falconer, R.A., Lin, B., 2007. Mathematical development and verification of a non-orthogonal finite volume model for groundwater flow applications. Adv. Water Resour. 30, 29–42.
McDonald, M.G., Harbaugh, A.W., 1988. A Modular Three-Dimensional Finite-difference Groundwater Flow Model: Techniques of Water-Resources Investigations of the United States Geological Survey, 586p (Book 6, Chapter A1).
Mehl, S., Hill, M.C., 2004. Three-dimensional local grid refinement method for block-centered finite-difference groundwater models using iteratively coupled shared nodes: a new method of interpolation and analysis of errors. Adv. Water Resour. 27 (9), 899–912.
Mendoza, C.A., Therrien, R., Sudicky, E.A., 1991. ORTHOFEM User's Guide Version 1.02. Waterloo Center for Groundwater Research, Univ. of Waterloo, Waterloo, On., Canada.
Niswonger, R.G., Prudic, D.E., 2004. Modeling variably saturated flow using kinematic waves in MODFLOW. In: Hogan, J.F., Phillips, F.M., Scanlon, B.R. (Eds.), Groundwater Recharge in a Desert Environment—The Southwestern United States: Washington, D.C., American Geophysical Union, Water Science and Application Series, vol. 9, pp. 101–112.
Niswonger, R.G., Prudic, D.E., Regan, R.S., 2006. Documentation of the Unsaturated-Zone Flow (UZF1) Package for Modeling Unsaturated Flow Between the Land Surface and the Water Table with MODFLOW-2005: U.S. Geological Survey Techniques and Methods, 6–A19, p. 62.
Pikul, M.F., Street, R.L., Remson, I., 1974. A numerical model based on coupled one-dimensional Richards and Boussinesq equations. Water Resour. Res. 10 (2), 295–302.
Sheikh, V., van Loon, E.E., 2007. Comparing performance and parameterisation of a 1D unsaturated zone model across scales. Vadoze Zone J. 6 (3), 638–650.
Sherlock, M.D., McDonnell, J.J., Curry, D.S., Zumbuhl, A.T., 2002. Physical controls on septic leachate movement in the vadose zone at the hillslope scale, Putnam County, New York, USA. Hydrol. Process. 16, 2559–2575.
Skaggs, R.W., 1978. A Water Management Model for Shallow Water Table Soils. Tech. Rep. 134. Water Resources Research Inst., North Carolina State Univ., Raleigh.
Sophocleus, M., Perkins, S.P., 2000. Methodology and application of combined watershed and groundwater models in Kansas. J. Hydrol. 236, 185–201.
Spitz, F.J., Nicholson, R.S., Daryll, A.P., 2001. A nested rediscretization method to improve pathline resolution by eliminating weak sinks representing wells. Ground Water 39 (5), 778–785.
Twarakavi, N.K.C., Šimůnek, J., Sophia, S., 2008. Evaluating interactions between groundwater and vadose zone using the HYDRUS-based flow package for MODFLOW. Vadose Zone J. 7 (2), 757–768.
van Genuchten, M.Th., 1980. A closed-form equation for predicting the hydraulic conductivity of unsaturated soils. Soil Sci. Am. J. 44, 892–898.
Vogel, T., Huang, K., Zhang, R., van Genuchten, M.Th., 1996. The HYDRUS Code for Simulating One-dimensional Water Flow, Solute Transport, and Heat Movement in Variably-saturated Media, Version 5.0, Research Report No. 140. U.S. Salinity Laboratory Agricultural Research Service U.S. Department of Agriculture Riverside, California.
Zhang, W.Z., 1983. Unsteady Groundwater Flow CALCULATION and Groundwater Resources Evaluation. Science Press, Beijing, China (in Chinese).
Zhu, Y., Yang, J.Z., Tong, J.X., 2010. A simplified 3D numerical model for groundwater flow in declining aquifer-aquitard system. J. Sichuan Univ. (Eng. Sci. Ed.) 42 (6), 43–50 (In Chinese).